

## DETERMINATION OF ELASTIC $T$ -STRESS ALONG THREE-DIMENSIONAL CRACK FRONTS USING AN INTERACTION INTEGRAL

TOSHIO NAKAMURA

Department of Mechanical Engineering, State University of New York at Stony Brook,  
NY 11794, U.S.A.

and

DAVID M. PARKS

Department of Mechanical Engineering, Massachusetts Institute of Technology, Cambridge,  
MA 02139, U.S.A.

(Received 18 July 1991; in revised form 31 October 1991)

**Abstract**—We introduce an effective computational method, based on an interaction integral, to evaluate elastic  $T$ -stress along three-dimensional crack fronts. Using this technique,  $T$ -stress distributions of various three-dimensional geometries are determined from finite element calculations. The computed results show that the through-thickness variation of  $T$ -stress along the crack front of edge-cracked plates is relatively small under both tension and bending load conditions. The deviation from the corresponding two-dimensional results increases with increasing relative crack length and with decreasing relative plate thickness. The increase in  $T$ -stress with decreasing thickness results from the inherent positive biaxiality of thin elastic plates. Furthermore, the value of three-dimensionally computed  $T$ -stress in these through-crack geometries increases with increasing Poisson's ratio. The  $T$ -stress distribution is also calculated along the curved crack front of a surface-flawed plate. For the particular geometry considered, the maximum  $T$ -stress along the crack front is located at the mid-point of the crack front, and there is a greater variation of  $T$ -stress along the crack front under bending loads than in tension.

### 1. INTRODUCTION

The so-called  $T$ -stress, or second term of the Williams (1957) series expansion for linear elastic crack-tip fields, has found many uses in fracture mechanics applications. Larsson and Carlsson (1973) and Rice (1974) showed that the sign and magnitude of the  $T$ -stress (relative to  $K_I/\sqrt{\pi a}$ ) substantially altered the size and shape of the plane strain crack-tip plastic zone at finite load levels corresponding to the ASTM limit of  $2.5 (K_I/\sigma_0)^2$  less than or equal to crack size, ligament length, etc., where  $\sigma_0$  is tensile yield strength.

Cotterell and Rice (1980) showed how the sign of the  $T$ -stress determines the stability of straight-ahead mode I cracking; cracks with  $T < 0$  are stable in this mode while those having  $T > 0$  are prone to curve off the initial crack plane.

Bilby *et al.* (1986) showed that the  $T$ -stress can strongly affect the magnitude of hydrostatic triaxiality in the very near tip elastic-plastic fields of a non-hardening material. More recently, Hancock and co-workers (Al-Ani and Hancock, 1991; Betegón and Hancock, 1991; Du and Hancock, 1991) have shown that the  $T$ -stress, in addition to the  $J$ -integral, provides a practical *two-parameter* characterization of plane strain elastic-plastic crack-tip fields in a variety of crack configurations and loadings. The important feature emerging from these works is that negative  $T$ -stress values can substantially reduce levels of crack-tip stress triaxiality, even under conditions of contained plastic flow, with larger reductions in triaxiality as  $T$  becomes more negative. The efficacy of this methodology in accurately describing crack-tip fields has also been demonstrated by O'Dowd and Shih (1991, 1992) in plane strain and by Parks and Wang (Parks, 1991a; Wang and Parks, 1990; Wang, 1991) in three-dimensional surface-cracked geometries. In short, these recent studies indicate that the value of the elastic  $T$ -stress, along with the  $J$ -integral or other measure of the scale of crack-tip deformation (e.g. CTOD), can provide exceptional improvement in the ability to describe local crack-tip stress triaxiality on the scale of fracture process zone

size (i.e. at distances from the tip of the order  $J/\sigma_0$  or CTOD), as compared to any single-parameter crack-tip description.

In order for the potential benefits of such an improved resolution in describing crack-tip fields to be realized in improved fracture mechanics analyses of engineering applications, much work is required in the construction and interpretation of experiments, and in micromechanics modeling of fracture (Parks, 1991b). However, an important basis for such a two-parameter fracture mechanics methodology rests upon the ability to calculate  $T$ -stress in essentially arbitrary crack configurations with relatively small levels of effort.

Two-dimensional studies (Larsson and Carlsson, 1973; Leever and Radon, 1983; Cardew *et al.*, 1984; Kfour, 1986; Sham, 1991) have shown that the  $T$ -stress depends strongly on the type of loading as well as on the relative crack length and overall geometry.

In the context of two-dimensional traction boundary problems in isotropic elasticity, the  $T$ -stress is independent of material elastic properties, as well as being independent of plate thickness (i.e. plane strain and plane stress  $T$ -values coincide). These features should not necessarily be expected within a three-dimensional context, but existing three-dimensional studies of the  $T$ -stress are far less extensive. Wang and Parks (1990) evaluated  $T$ -stress distributions along semi-elliptical surface crack fronts by subtracting the dominant singular terms from very detailed three-dimensional finite element solutions, as well as by developing simplified evaluations of  $T$ -stress distributions based on the line-spring model. Wang (1991) used these  $T$ -stress distributions in quantitatively predicting the varying triaxiality of elastic-plastic crack front stress fields in shallow and deep surface crack geometries subjected to both tension and bending loading.

Here we develop a general computationally-effective method for extracting  $T$ -stress distributions along three-dimensional crack fronts from moderately detailed finite element solutions; two-dimensional and axisymmetric geometries emerge as special cases. The method, based on an interaction integral, generalizes a two-dimensional method for  $T$ -stress evaluation given by Kfour (1986). Computational implementation of the method is based on standard domain integral techniques. Several applications of the method illustrate some inherently three-dimensional aspects of the  $T$ -stress, including dependence on the Poisson ratio and relative plate thickness.

## 2. EXTRACTION OF $T$ ALONG A THREE-DIMENSIONAL CRACK FRONT

### 2.1. Near tip field and line-load solutions

In an isotropic linear elastic body containing a crack subject to symmetric (mode I) loading, the leading terms [up to order  $\mathcal{O}(1)$ ] in a series expansion of the stress field very near the crack front are

$$\begin{aligned} \sigma_{11} &= \frac{K_I}{\sqrt{2\pi r}} \cos \frac{\theta}{2} \left( 1 - \sin \frac{\theta}{2} \sin \frac{3\theta}{2} \right) + T, & \sigma_{22} &= \frac{K_I}{\sqrt{2\pi r}} \cos \frac{\theta}{2} \left( 1 + \sin \frac{\theta}{2} \sin \frac{3\theta}{2} \right) \\ \sigma_{33} &= \frac{K_I}{\sqrt{2\pi r}} 2\nu \cos \frac{\theta}{2} + T_{33}, & \sigma_{12} &= \frac{K_I}{\sqrt{2\pi r}} \sin \frac{\theta}{2} \cos \frac{\theta}{2} \cos \frac{3\theta}{2}, & \sigma_{13} &= \sigma_{23} = 0, \end{aligned} \quad (1)$$

where  $r$  and  $\theta$  are the in-plane coordinates of the plane normal to the crack front,  $K_I$  is the local stress intensity factor, and  $\nu$  is the Poisson's ratio. Here  $x_1$  is the direction formed by the intersection of the plane normal to the crack front and the plane tangential to the crack plane. The terms  $T$  ( $=T_{11}$ ) and  $T_{33}$  are the amplitudes of the second order terms in the three-dimensional series expansion of the crack front stress field in the  $x_1$  and  $x_3$  directions, respectively. Under general loading conditions, there may also be a constant  $T_{13}$ -term present (Parks, 1991a), but we do not consider this case further. For later use, we find it convenient to additively decompose the stress component  $T_{33}$  into the form  $T_{33} = \sigma^* + \nu T$ . This permits the identification of  $\sigma^*$  with a state of simple tension tangent to the crack front causing crack front extensional strain  $\epsilon_{33} = \sigma^*/E$  and Poisson contractions  $-\nu\sigma^*/E$  in the

$x_1$  and  $x_2$  directions. (Here  $E$  is Young's modulus.) Under two-dimensional plane strain conditions ( $\epsilon_{33} = 0$ ), we have  $\sigma^* = 0$ .

For the purpose of extracting the  $T$ -stress distribution along the crack front of a stressed body, we make use of an auxiliary solution corresponding to a plane strain line-load applied along the crack front. The solution is the special case of a line-load symmetrically applied at the apex of a wedge of included angle  $2\pi$  (Timoshenko and Goodier, 1970). Suppose that a line-load with magnitude  $f$  (force per unit length) in the  $x_1$  direction is locally applied along the same crack front segment. Then the stress field in the crack-tip region is given by

$$\begin{aligned} \sigma_{11}^L &= \frac{f}{\pi r} \cos^3 \theta, & \sigma_{22}^L &= \frac{f}{\pi r} \cos \theta \sin^2 \theta, & \sigma_{33}^L &= \frac{f}{\pi r} \nu \cos \theta \\ \sigma_{12}^L &= \frac{f}{\pi r} \cos^2 \theta \sin \theta, & \sigma_{13}^L &= \sigma_{23}^L = 0. \end{aligned} \tag{2}$$

Here, the superscript "L" designates the field as that of the line-load solution. The stress field (2) also admits compatible strain ( $\epsilon_{ij}^L$ ) and displacement ( $u_i^L$ ) fields. The above solutions are valid at any material point as long as  $r$ , its radial distance to the crack front, is sufficiently small compared to other relevant physical dimensions (e.g. crack front radius of curvature, distance to free surface, etc.).

2.2. Interaction integral

In order to extract the elastic  $T$ -term, an interaction integral is introduced. The interaction integral shown here is similar to that used to evaluate mixed-mode stress intensity factors along a three-dimensional crack front (Nakamura and Parks, 1989).

We begin by considering the line-load,  $f_i = f\mu_i(s)$ , to be applied along the crack front as shown in Fig. 1(a). In the figure,  $s$  is an arc-length measuring parameter representing the location of the crack-tip on the crack front, and  $\mu_i(s)$  is a unit vector giving the direction formed by the intersection of the plane normal to the crack front and the plane tangential

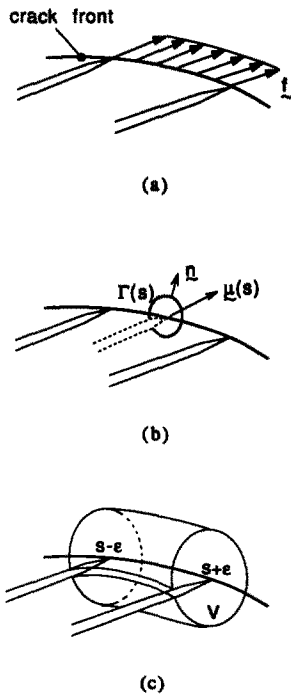


Fig. 1. (a) Line-load applied in the direction of crack advance along the crack front. (b) Crack tip contour  $\Gamma$  on the plane locally perpendicular to the crack front where  $s$  represents the location of the crack tip. (c) Volume  $V$  which encloses the crack front segment where  $I$  is evaluated.

to the crack front at  $s$ . Suppose we superimpose the near tip field (1) with the field due to the line-load application (2). We can introduce a local conservation integral as

$$I(s) = \lim_{\Gamma \rightarrow 0} \mu_k(s) \int_{\Gamma(s)} \left[ \sigma_{ij} \varepsilon_{ij}^L n_k - \sigma_{ij} \frac{\partial u_i^L}{\partial x_k} n_j - \sigma_{ij}^L \frac{\partial u_i}{\partial x_k} n_j \right] d\Gamma. \quad (3)$$

Here, a path  $\Gamma$  where the integral is evaluated surrounds the crack front at  $s$  and lies in the plane perpendicular to the crack front at  $s$ . The components  $n_i$  are those of a unit vector, lying in this plane and normal to the tangent to  $\Gamma$ , as shown in Fig. 1(b). Note that the limit ( $\Gamma \rightarrow 0$ ) must be preserved in three-dimensional problems. However, the shape of the path may be arbitrary as  $\Gamma$  shrinks onto the tip.

Now suppose that  $\mu_i(s)$  is given in the local  $x_1$  direction and that the path  $\Gamma$  is circular with radius  $r$ . Then as the limit is taken ( $r \rightarrow 0$ ), the stress fields in (1) and (2) (and their associated kinematic fields) become applicable in the integrand. After substituting these fields into the integral and performing tedious but routine algebra, the interaction integral may be evaluated as

$$I(s) = \frac{f}{E} [T(s)(1 - \nu^2) - \nu \sigma^*(s)]. \quad (4)$$

In the integration, the terms in the crack-tip fields (1) containing  $K_I$  cancel out exactly, and only the non-singular terms in (1) contribute to  $I(s)$ . Using the relation  $\sigma^*(s) = E\varepsilon_{33}(s)$  noted above, and solving for  $T(s)$ , we obtain,

$$T(s) = \frac{E}{f(1 - \nu^2)} [I(s) + \nu \varepsilon_{33}(s)]. \quad (5)$$

Under two-dimensional plane strain conditions,  $\varepsilon_{33} = 0$ , and the formulation leading to (5) is similar to that given by Kfoury (1986). Finally, if we evaluate (3) using the computed stress ( $\sigma_{ij}$ ) and deformation ( $u_i$ ) field of a boundary value problem and the exact auxiliary solution of the line-load (2), with unit magnitude ( $f = 1$ ), then the local value of  $T$ -stress at the crack front point  $s$  in the boundary value problem can be determined.

In numerical analyses, the expression (3) is not suitable for evaluating  $I(s)$  since accurate numerical evaluation of limiting fields along the crack front is difficult. Here the so-called "domain integral formulation" (Li *et al.*, 1985; Shih *et al.*, 1986) is adopted. With the aid of the spatial weighting function,  $q_k$ , and the divergence theorem, the integral over a domain/volume is,

$$\begin{aligned} \bar{I}(s) &= \int_{s-\varepsilon}^{s+\varepsilon} q_l(s') \mu_l(s') I(s') ds' \\ &= \int_{V(s)} \left[ \left( \sigma_{ij} \frac{\partial u_i^L}{\partial x_k} + \sigma_{ij}^L \frac{\partial u_i}{\partial x_k} \right) \frac{\partial q_k}{\partial x_j} - \sigma_{ij} \varepsilon_{ij}^L \frac{\partial q_k}{\partial x_k} \right] dV. \end{aligned} \quad (6)$$

Here  $V(s)$  is a volume which encloses the crack front segment bounded by  $s - \varepsilon$  and  $s + \varepsilon$  as shown in Fig. 1(c). In a finite element model, the distance  $\varepsilon$  is usually taken as the length of element layer adjoining the crack front. An appropriate generalization of (6), applicable to cases for which body force and thermal strain are present, is given in the Appendix. A simple approximation to  $I$  is obtained by assuming that its variation is nearly linear within the segment. Then its centroidal value can be calculated as,

$$I(s) \doteq \bar{I}(s) \left/ \int_{s-\epsilon}^{s+\epsilon} q_i(s') \mu_i(s') ds' \right. \quad (7)$$

More detailed and consistent procedures for determining  $I(s)$  exist. However our computational experiences have shown that the approximate method of (7) provides preferable results for the analysis when the accuracy of  $\bar{I}$  cannot be uniformly obtained along the entire crack front ; i.e. when very steep gradients in  $I(s)$  exist, as occurs near the intersection of a crack front with a free surface. This discussion of finite element implementation of domain integral methods is brief ; more details can be found in Nakamura and Parks (1989) and in Li *et al.* (1985).

### 3. SINGLE EDGE-CRACKED PLATES

#### 3.1. Model

For the initial three-dimensional model, a single edge-cracked plate (ECP) containing a straight through-crack is considered. The specimen is subjected to either remote tension or bending as shown in Fig. 2. For the tension case, a constant normal stress  $\sigma^\infty$  is applied on the end planes of the plate. For the bending case, a linearly-varying tensile stress, with the largest value (maximum bending stress)  $\sigma^\infty$ , is applied on the top and bottom planes. In the model, the ratio of half-height,  $H$ , to the width,  $W$ , is chosen to be  $H/W = 2$ . Two families of geometries are considered, through variations in crack length,  $a$ , and plate thickness,  $t$ . The Poisson's ratio varies over the range  $0 \leq \nu \leq 0.499$ . The coordinates are chosen so that  $x_1$  is in the crack advance direction,  $x_2$  is in the axial direction of the plate and the  $x_3$  axis is the crack front. The origin is located at the mid-point of the crack front.

In constructing the finite element mesh, we have used the symmetry conditions across the mid-plane ( $x_3/t = 0$ ) and the crack and ligament plane ( $x_2/t = 0$ ). Different meshes are used for geometries with different crack lengths and thickness. In all our models, the element size is gradually decreased as the radial distance to the crack front decreases, while the angular increment of each mesh is kept constant in the crack front region. The identical planar mesh is repeated along the  $x_3$  axis. Since a high stress gradient along the crack front is expected near the free-surface, thinner elements are employed away from the mid-plane.

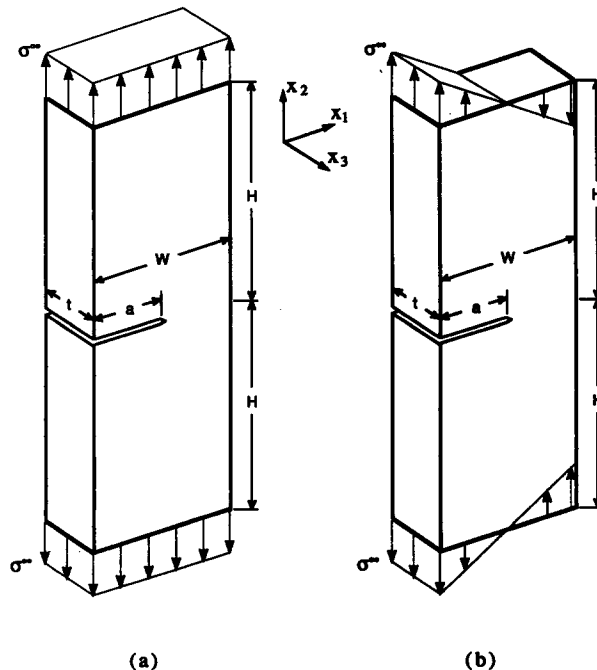


Fig. 2. Schematic of three-dimensional single edge-cracked plate under (a) tension and (b) bending.

The number of element layers through the half-thickness is 8. A total of approximately 1200 20-noded three-dimensional quadratic elements with reduced integration ( $2 \times 2 \times 2$ ) are used to construct the quarter-model.

### 3.2. Effects of Poisson's ratio

In contrast to the case of two-dimensional (plane strain or plane stress) traction boundary value problems, in three dimensions the local  $T$ -stress is influenced by the value of Poisson's ratio. (Three-dimensional distributions of stress intensity factor also depend on  $\nu$  in these geometries.) Using an ECP with fixed geometry given by ( $a/W = 0.5$ ,  $t/W = 0.5$ ), several computations were carried out for different Poisson's ratios under both tension and bending. In determining the  $T$ -stress from the finite element solution,  $\bar{I}$  is computed over several domains/volumes enclosing each crack front node. Then the average value is taken and  $I$  is obtained from (7). Finally, the relation (5) is used to calculate  $T$  from  $I$  and  $\varepsilon_{33}$  at the crack front node.

Before discussing the numerical results, we note that the accuracy of  $T$  is influenced by several factors. First, in cases when the interaction integral is positive,  $T$  is calculated from the *difference* in the magnitudes of  $|I|$  and  $|\varepsilon_{33}|$ , since  $\varepsilon_{33}$  is usually negative along the crack front. This could be a potential source of significant error, especially when the difference of the terms is small compared to their magnitude. Next, in this analysis,  $\varepsilon_{33}(s)$  at a crack front node is obtained from the tangential displacement components at neighboring crack front nodes using the quadratic shape functions. This method requires a very small element (in the  $r$  direction) along the crack front to compute a sufficiently accurate value for  $\varepsilon_{33}$ . In our computations, the radius of the first ring of elements wrapped about the crack front,  $r_{\min}$ , always satisfied  $r_{\min} < 0.001 \times l$ , where  $l = \min[a, W - a, t]$ . We expect that this provides estimates of  $\varepsilon_{33}$  which are accurate to 2~3% of the exact value. However, when the magnitude of  $\varepsilon_{33}$  is very large, such as near the intersection of the crack front with a free-surface, the accuracy with which  $\varepsilon_{33}$  is computed must deteriorate. Moreover, at such locations, we might expect that (corner) singular values of  $\varepsilon_{33}$  would cause  $\bar{I}$  to diverge.

The  $T$ -stress along the half-crack front, normalized by  $\sigma^\infty$ , is shown in Fig. 3. Figure 3(a) shows the results from the tension case. For each Poisson's ratio, the through-thickness variation remains small except in the region near the free-surface,  $x_3/t > 0.4$ . The  $T$ -stress increases essentially uniformly across the crack front with increasing Poisson's ratio, becoming positive for a nearly incompressible plate. The case of  $\nu = 0$  is equivalent to the two-dimensional solution (plane strain and plane stress conditions). Near the mid-plane ( $x_3/t = 0$ ), there is a difference of approximately  $\sigma^\infty/2$  between the  $T$ -stress for the cases  $\nu = 0.499$  and  $\nu = 0$  [or the two-dimensional solution; Sham (1991)]. The results of the bending case are shown in Fig. 3(b). The  $T$ -stress distributions are similar to those of tension, except all the values are positive, and the sensitivity to the value of Poisson's ratio is somewhat smaller.

### 3.3. Various crack lengths

Next, the effects of crack length are studied by computing mid-plane  $T$ -stress values for various relative crack depths ranging from  $0.1 \leq a/W \leq 0.7$ . The relative thickness of the plate and the Poisson's ratio are fixed at  $t/W = 0.5$  and  $\nu = 0.3$ , respectively. The  $T$ -stress is normalized by  $\sigma^\infty$  in Fig. 4(a) and by  $K_I/\sqrt{\pi a}$  in Fig. 4(b), the latter being a normalization more commonly used in two-dimensional studies. The normalizing stress intensity factor  $K_I$  is the local value at mid-plane, as computed independently from three-dimensional domain integral evaluation of the crack-front distribution of  $J$ . This method has been successfully employed in many three-dimensional analyses [see, for example, Nakamura and Parks (1989)]. Both tension and bending cases show increasing  $T$ -stress at mid-plane for longer crack lengths. This trend has been used extensively by Al-Ani and Hancock (1991) in explaining systematic variations in elastic-plastic crack-tip constraint for plane strain edge-cracks of varying depths under tension and bending. As compared to

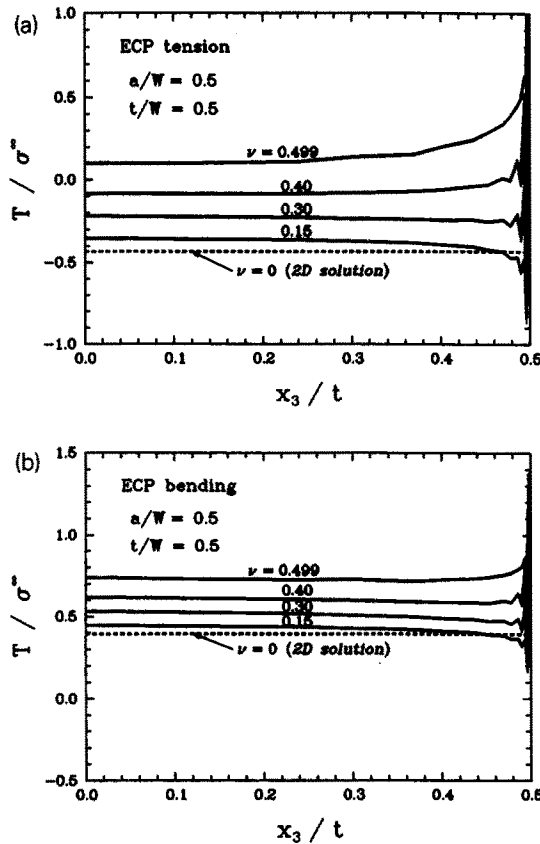


Fig. 3. Variation of normalized  $T$ -stress along the crack front of an edge-cracked plate for various Poisson's ratios under (a) tension and (b) bending.

the corresponding two-dimensional solutions (Sham, 1991), the three-dimensional normalized  $T$ -stress values are always slightly higher, except for the shallow cracks ( $a/W < \sim 0.2$ ) under bending when  $T$  is normalized by  $\sigma^\infty$ .

### 3.4. Effects of plate thickness

The effect of the relative plate thickness on the three-dimensional  $T$ -stress distributions is studied by using finite element models having similarly-arranged in-plane meshes, but with differing plate thicknesses. The radial extent of the elements adjacent to the crack front is kept sufficiently small relative to the thickness. The models were subjected to in-plane loading uniformly distributed through the thickness. For this analysis, the relative crack depth and Poisson ratio are fixed at  $a/W = 0.5$  and  $\nu = 0.3$ , respectively, and the straight crack front intersects the free-surfaces orthogonally.

Before discussing the numerical results, we note that in problems of this sort, the local stress intensity factor  $K_I$  in general varies along the crack front. When thickness  $t$  becomes large compared to in-plane dimensions (e.g. crack length  $a$ ), this variation should approach

$$K_I(x_3/t, \nu) = K_I^{2D} \quad \text{as } t/a \rightarrow \infty, \quad (8)$$

where  $K_I^{2D}$  is the plane strain stress intensity factor for this in-plane geometry and load per unit thickness. In this case, the stress intensity factor is uniform except in the small region near the free-surfaces ( $|x_3/t| = 0.5$ ) where the corner field prevails and  $K_I$  must vanish (Nakamura and Parks, 1988). As thickness becomes small with respect to in-plane dimensions, the stress intensity factor distribution for a thin plate tends to

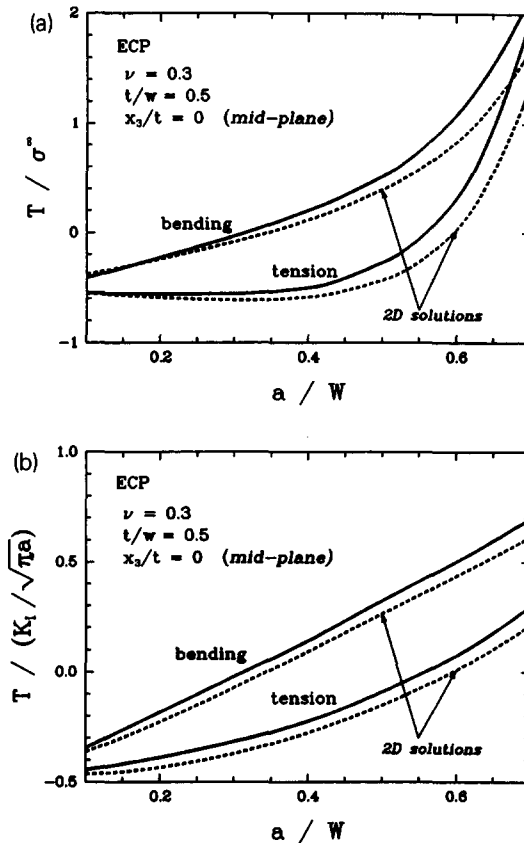


Fig. 4. Mid-plane value of  $T$ -stress as a function of crack length in edge-cracked plates.  $T$  is normalized by (a)  $\sigma^\infty$  and (b)  $K_I/\sqrt{\pi a}$ . Two-dimensional solutions (Sham, 1991) are also shown.

$$K_I(x_3/t, \nu) = k(x_3/t, \nu) K_I^{2D} \quad \text{as } t/a \rightarrow 0. \quad (9)$$

In (9),  $K_I^{2D}$  is the plane stress solution to the boundary value problem. [In traction boundary value problems, the plane stress value of  $K_I^{2D}$  in (9) coincides with the plane strain value of  $K_I^{2D}$  in (8).] The dimensionless function  $k$  in (9) is independent of any remote loading conditions and in-plane dimensions. Its variation along the crack front for various Poisson's ratios is shown in Nakamura and Parks (1988). The function  $k$  is of order unity except near the free surface ( $k \rightarrow 0$  as  $|x_3/t| \rightarrow 0.5$  for  $\nu \neq 0$ ) and peaks at mid-plane. For  $\nu = 0$ ,  $k$  is identically unity. For given in-plane geometry and loading, when relative plate thickness  $t/a$  is neither "thick" nor "thin", the through-thickness variation of  $K_I$  increases with decreasing thickness until reaching the thin plate limit (9) at sufficiently small values; say,  $t/a \leq 0.1$ . Alternatively, the through-thickness variation tends to become more uniform as thickness increases, effectively reaching the thick plate limit (8) at sufficiently large values; say,  $t/a \geq 10$ .

The thickness-dependence of the  $T$ -stress distribution can be expressed in a similar manner. When the thickness is large,

$$T(x_3/t, \nu) = B^{2D} \frac{K_I^{2D}}{\sqrt{\pi a}} \equiv T^{2D} \quad \text{as } t/a \rightarrow \infty, \quad (10)$$

where  $B^{2D}$  is a dimensionless "biaxiality" parameter depending (as does  $K_I^{2D}$ ) only on in-plane geometry and loading. Values of  $B^{2D}$  have been tabulated for several crack geometries (Larsson and Carlsson, 1973; Levers and Radon, 1983; Cardew *et al.*, 1984; Kfoury, 1986; Sham, 1991).



From considerations of superposition and dimensional analysis, we propose that, as relative thickness diminishes in the boundary value problem posed, the through-thickness variation of  $T$ -stress can be expressed as

$$T(x_3/t, \nu) \simeq T^{2D} + B^{\text{thin}}(x_3/t, \nu) \frac{K_I(x_3/t, \nu)}{\sqrt{\pi t}}. \tag{11}$$

Here we again exploit the equivalence of the plane stress and plane strain two-dimensional solutions for  $T^{2D}$ . In this sense,  $T^{2D}$  represents the “remote” value which applies in the plane stress field found at radii large compared to thickness  $t$ , but small compared to crack length  $a$ . The function  $B^{\text{thin}}$  represents the local biaxiality factor of a thin plate, which will be more fully described below. Although we have motivated the functional form of (11) from the perspective of small relative thickness, we might anticipate a broader range of applicability since the thick plate result (10) is recovered as  $t \rightarrow \infty$  at fixed in-plane dimensions.

Figure 5 shows larger mid-plane  $T$ -stress in thinner plates under both tension and bending loads. As the plate thickness increases, the normalized  $T$ -stress decreases and approaches the two-dimensional solution. The three-dimensional results nearly merge with the two-dimensional solution for plates with  $t/W > 0.1$ , aside from the slight differences caused by the Poisson’s ratio effect shown in Fig. 3. However, the relatively strong effect of increasing  $T$ -stress with decreasing plate thickness shown in Fig. 5 is perhaps unexpected, especially considering that  $T$  is still markedly increasing at intuitively “small” thicknesses,  $t/W \leq 0.001$ .

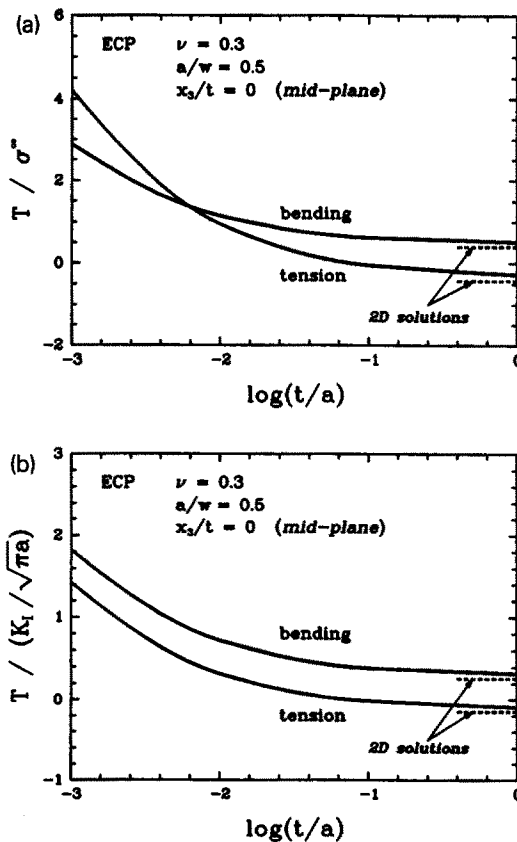


Fig. 5. Mid-plane value of  $T$ -stress as a function of plate thickness in edge-cracked plates.  $T$  is normalized by (a)  $\sigma^\infty$  and (b)  $K_I/\sqrt{\pi a}$ . Two-dimensional solutions (Sham, 1991) are also shown.

The explanation for this phenomenon lies in the inherent biaxiality parameter for a "thin elastic plate" as considered by Nakamura and Parks (1988). They analysed a three-dimensional domain of thickness  $t$  and radius  $R \gg t$ . They applied the in-plane traction calculated from the plane stress fields of (1) (i.e.  $\sigma_{33} = 0$ ) at the outer radius  $R$ , with remote amplitude  $K^{\text{far}} = K_1^{2D}$ . Their solution provided the full three-dimensional fields within the domain  $r < R$ . Although the remote plane stress  $K$ -field loading of the thin disk has no applied  $T$ -stress (i.e.  $T^{2D} = 0$ ), on dimensional grounds we expect that *locally* there exists along the thin plate crack front a  $T$ -stress distribution

$$T(x_3/t, \nu) = B^{\text{thin}}(x_3/t, \nu) \frac{K_1(x_3/t, \nu)}{\sqrt{\pi t}} \quad \text{as } t/a \rightarrow 0, \quad (12)$$

where from (9), the three-dimensional variation of local plane strain stress intensity factor in the thin plate is given by  $K_1(x_3/t, \nu) = k(x_3/t, \nu)K^{\text{far}}$ , and the function  $B^{\text{thin}}$  is the (inherent) biaxiality parameter for a thin plate, independent of any loading conditions. Since the remote plane stress field is also exact in the three-dimensional case for  $\nu = 0$ ,  $B^{\text{thin}}(x_3/t, 0) \equiv 0$ .

We have applied the interaction integral to the thin plate solutions of Nakamura and Parks (1988), and Fig. 6 shows the dimensionless biaxiality function  $B^{\text{thin}}$ . At mid-plane  $T$  increases with increasing  $\nu$ . The through-thickness variation of  $T$  is somewhat stronger than that seen in Fig. 3.

Returning to the thickness-dependence of mid-plane  $T$ -stress shown in Fig. 5, we see that the superposition shown in (11) can indeed be treated as an approximate interpolation for  $T$  applicable to cases when the plate is neither thick nor thin. With the use of (8)–(10) and (12), the normalized  $T$  in (11) can also be expressed as

$$\frac{T(x_3/t, \nu)}{K_1(x_3/t, \nu)/\sqrt{\pi t}} \approx \sqrt{\frac{t}{a}} B^{2D} + B^{\text{thin}}(x_3/t, \nu). \quad (13)$$

For a thick plate, the first term on the right-hand side of (13) dominates, while it vanishes for a thin plate. In Fig. 7, using known calibrations of  $B^{2D}$ -values for edge-cracked specimens under tension and bending (Sham, 1991) and the mid-plane value of  $B^{\text{thin}}(0, \nu = 0.3) = 0.045$  from Fig. 6, the approximate thickness-dependence of  $T$  at the mid-plane as given by (11) or (13) is plotted for the relative thickness range  $0.001 \leq t/a \leq 1$ . In the same figure, the full-field solution [replot of Fig. 5(b)] is also shown. As expected, the accuracy of (13) is very high for plates of small relative thickness. In the intermediate thickness regime ( $0.01 < t/a < 1.0$ ), the agreement with the full-field solution is also very good. We have

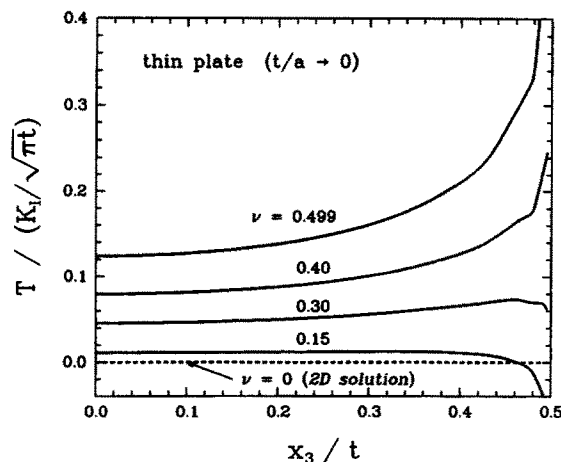


Fig. 6. Variation of normalized  $T$ -stress along the crack front in a thin elastic plate.

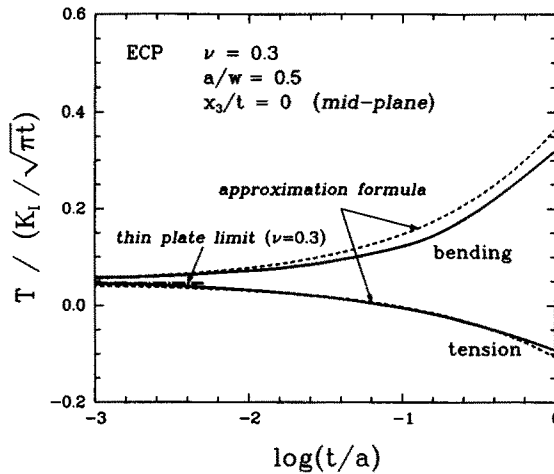


Fig. 7. Mid-plane variation of normalized  $T$ -stress in edge-cracked plates as a function of relative plate thickness,  $t/a$ , showing the coincidence of biaxiality with  $B^{\text{thin}}$  under both tension and bending as  $t/a \rightarrow 0$ . Dashed lines represent the approximate thickness-dependence of  $T$ -stress obtained from (11).

also used (13) to approximate  $T$ -stress with different Poisson's ratio plates at various crack front positions. The results show that even with the nearly incompressible plate ( $\nu = 0.499$ ), the difference,  $\Delta T$ , between the full-field solution and the approximate  $T$ -stress always satisfies  $|\Delta T| < 0.05 (K_I / \sqrt{\pi t})$ , except at crack front positions very close to the free-surface. Thus the approximation formula provides an excellent estimate of  $T$ -stress along the crack front of through-cracked plates of any relative thickness.

The implications of thickness-dependence for the  $T$ -stress in three-dimensional through-cracked plates would seem to be profound; as seen in Figs 5 and 7, geometries having negative  $T$ -stress as calculated two-dimensionally ( $B^{2D} < 0$ ) can in fact develop positive  $T$ -stress providing  $\sqrt{t/a} < \sim B^{\text{thin}} / |B^{2D}|$ .

#### 4. SURFACE CRACK MODEL

##### 4.1. Model

In order to test the interaction integral on a non-straight crack front, the  $T$ -stress distribution of a surface crack is computed. The surface-flawed plate contains a semi-elliptical shaped crack and is subjected to either remote tension or bending loads as shown by a quarter model in Fig. 8. The dimensions of the plate, relative to plate thickness  $t$ , are the half-height  $H/t = 8$ ; the half-width  $W/t = 4$ ; the mid-plane crack depth  $a/t = 0.6$ ; and the surface crack half-length  $c/t = 2.25$ , resulting in surface crack aspect ratio of  $a/c = 0.24$ . The parameter  $\phi$  represents the crack front location along a semi-elliptical crack front by measuring the angle to a corresponding point on an inscribed circle of radius  $a$ , as shown in the figure. The quarter-model of finite element mesh is constructed with 4960 8-noded linear elements. The computations are carried out for Poisson's ratios of  $\nu = 0$  and 0.3.

##### 4.2. Computed results

Figure 9 shows the variations of normalized  $K_I$  along the crack front. The results are close to other previously published results; e.g. Raju and Newman (1979). The  $T$ -stress is again computed along the crack front using the interaction integral. In this model,  $\varepsilon_{33}$  is taken as the local tangential strain along the crack front. In general, the computed results show that the domain dependence of  $\bar{I}$  over several different domains is somewhat greater than that of  $J$ , although the determination of the accuracy or the domain dependence of  $\bar{I}$  is difficult when its value is close to zero (see the discussion in Section 3.2).

The  $T$ -stress normalized by  $\sigma^\infty$  is shown in Fig. 10(a). The change in  $T$ -stress distribution attributable to the difference in Poisson ratio is smaller than the range of  $T$  along the crack front at fixed  $\nu$ . In addition, there is a much greater range of  $T$ -stress values along the crack

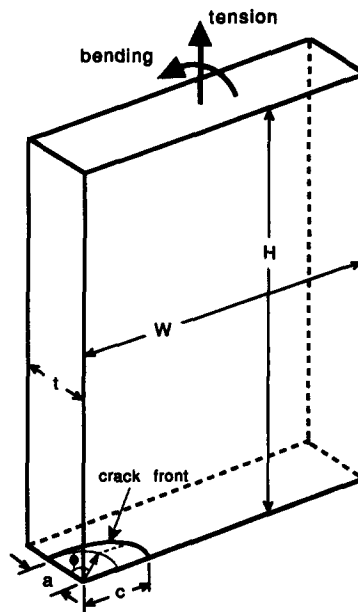


Fig. 8. Schematic of a quarter of a surface crack model under tension and bending. The location of a point along the crack front is parametrically expressed by the angle  $\phi$ .

front under bending than under tension. We note that values near the free-surface ( $\phi > 70^\circ$ ) may not be very accurate due to insufficient mesh refinement in that region. However, for surface cracks of the current aspect ratio ( $a/c = 0.24$ ), the physical extent of the crack front within  $70^\circ < \phi < 90^\circ$  is *much smaller* than that within  $0^\circ < \phi < 70^\circ$ . Figure 10(b) shows  $T$  normalized by  $K_I/\sqrt{\pi a}$ , where  $K_I$  is local stress intensity factor, as shown in Fig. 10(a). With this normalization, the variation of  $T$  along the crack front is reduced, due to the similar variations of  $K_I$  and  $T$  along the crack front, as shown in Figs 9 and 10(a).

The  $T$ -stress distributions shown in Fig. 10 are in good agreement with those determined by Wang and Parks (1990). These authors analysed several surface crack geometries using very detailed three-dimensional meshes, extracting  $T$  by subtracting the dominant singular term from the numerically-computed crack front stress fields. They also applied the simple line-spring model to obtain approximate distributions of  $T$ . At the center line ( $\phi = 0$ ) of a tensile-loaded plate of this geometry having  $\nu = 0.3$ , Wang and Parks obtained values of  $T/\sigma^\infty$  equal to  $-0.65$  and  $-0.60$  from the continuum and line-spring solutions,

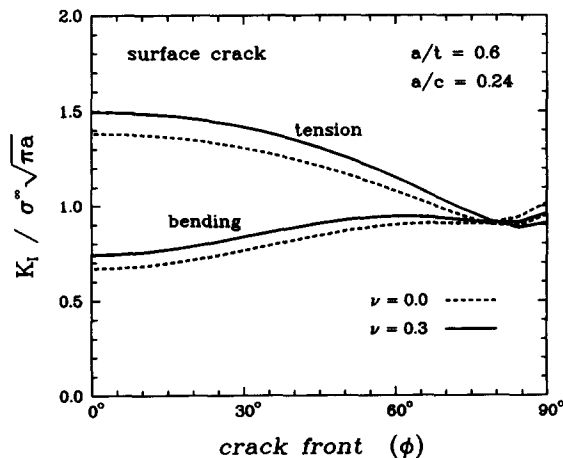


Fig. 9. Variation of local  $K_I$  along the crack front in a surface-cracked plate under remote tension and bending loads. Results are shown for Poisson ratios of  $\nu = 0$  and  $0.3$ .

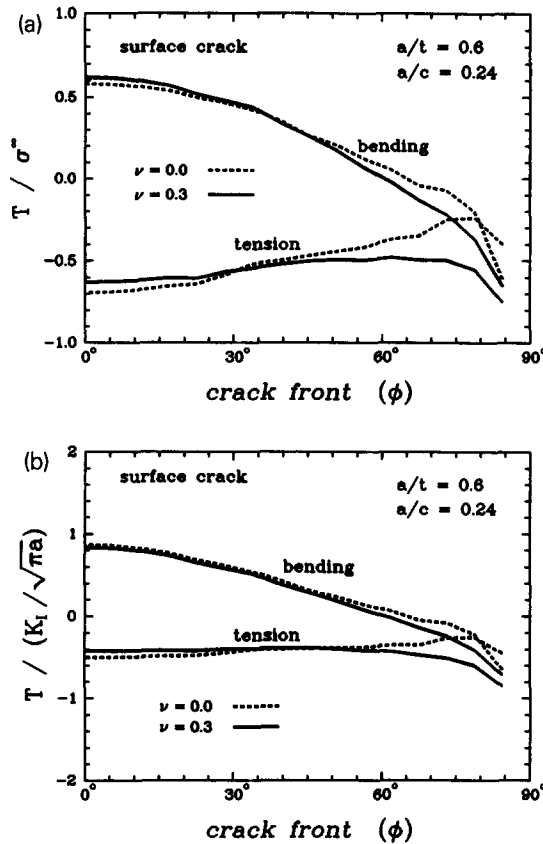


Fig. 10. Variation of  $T$ -stress along the crack front in a surface-cracked plate. Values of  $T$  are normalized by (a)  $\sigma^\infty$  and (b)  $K_I/\sqrt{\pi a}$ .

respectively, while the current method gives  $-0.62$ . Similarly, for bending loading, Wang and Parks obtained normalized  $T$ -stress values of  $0.51$  (continuum) and  $0.47$  (line-spring), while the current method gives  $0.61$ . All three of the solutions show only a very slight increase in  $T$  along most of the crack front ( $\phi < \sim 60^\circ$ ) for tension, and a sharp decrease with increasing  $\phi$  for bending, crossing zero at  $\phi \doteq 60^\circ$ .

### 5. DISCUSSION

We have introduced a general, accurate method to compute the non-singular  $T$ -stress along three-dimensional crack fronts from finite element solutions of moderate mesh refinement. Previous studies, based on specialized numerical techniques of more limited applicability, have presented  $T$ -stress solutions for various two-dimensional plate geometries, crack lengths and loading conditions. In three-dimensional geometries, the value of the  $T$ -stress is also influenced by the Poisson's ratio as well as the relative plate thickness.

We have shown that the superposition of the two limiting solutions, the thick and thin cases, gives a good approximation to the three-dimensional  $T$ -stress of a through-cracked plate. An intriguing implication of the inherently positive biaxiality parameter of thin plates suggests itself. As noted above, *all* such crack geometries develop positive  $T$ -stress at sufficiently small relative thickness providing only that  $K_I > 0$ . Cotterell and Rice (1980) showed that, within a two-dimensional planar framework, straight-ahead mode I cracking under positive  $T$ -stress was not stable with respect to small off-plane perturbations of the crack tip. We presume that similar inferences could be made in a three-dimensional context for off-plane perturbations of a segment of crack front, though precise calculations would be required.

On the fact of it, such a phenomenon would suggest that there exists, effectively, a

limiting relative thickness (or, for fixed thickness, a limiting crack extension) for which straight-ahead mode I cracking is not stable, regardless of in-plane geometry and loading. However, the inherently positive local  $T$ -stress we have identified is a three-dimensional feature of *planar* cracks in thin plates, and it is not clear if and how such fields would be altered as the scale of out-of-plane crack perturbation becomes significant with respect to plate thickness. It is conceivable that the amplitude of the positive thin plate  $T$ -stress effect could diminish with out-of-plane perturbation, so that the overall stability of the crack path would remain determined by the sign of  $T^{2D}$ , as originally formulated by Cotterell and Rice. These speculations would merit closer experimental and analytical study.

*Acknowledgements*—DMP acknowledges the support of the Office of Basic Energy Sciences, Department of Energy, under Grant No. DE-FG02-85ER13331. The authors gratefully acknowledge Dr Y.-Y. Wang of M.I.T. for providing us with the finite element mesh of the surface crack. The computations were performed on a VAXstation 3500 at the State University of New York at Stony Brook. The finite element analysis was carried out with the ABAQUS code, which was made available under academic license from Hibbit, Karlsson and Sorensen, Inc., Providence, RI.

## REFERENCES

- Al-Ani, A. M. and Hancock, J. W. (1991).  $J$ -dominance of short cracks in tension and bending. *J. Mech. Phys. Solids* **39**, 23–43.
- Betegón, C. and Hancock, J. W. (1991). Two-parameter characterization of elastic–plastic crack-tip fields. *J. Appl. Mech.* **58**, 104–110.
- Bilby, B. A., Cardew, G. E., Goldthorpe, M. R. and Howard, I. C. (1986). A finite element investigation of the effect of specimen geometry on the fields of stress and strain at the tip of stationary cracks. In *Size Effects in Fracture*, pp. 37–46. Institution of Mechanical Engineers, London.
- Cardew, G. E., Goldthorpe, M. R., Howard, I. C. and Kfoury, A. P. (1984). On the elastic  $T$ -term. In *Fundamentals of Deformation and Fracture (Eshelby Memorial Symposium)* (Edited by K. J. Miller and B. A. Bilby), pp. 465–476. Cambridge University Press, Cambridge.
- Cotterell, B. and Rice, J. R. (1980). Slightly curved or kinked cracks. *Int. J. Fract.* **16**, 155–169.
- Du, Z.-Z. and Hancock, J. W. (1991). The effect of non-singular stresses on crack-tip constraint. *J. Mech. Phys. Solids* **39**, 555–567.
- Kfoury, A. P. (1986). Some evaluations of the elastic  $T$ -term using Eshelby's method. *Int. J. Fract.* **30**, 301–315.
- Larsson, S. G. and Carlsson, A. J. (1973). Influence of non-singular stress terms and specimen geometry on small-scale yielding at crack tips in elastic–plastic material. *J. Mech. Phys. Solids* **21**, 263–278.
- Leevers, P. S. and Radon, J. C. (1983). Inherent stress biaxiality in various fracture specimen geometries. *Int. J. Fract.* **19**, 311–325.
- Li, F. Z., Shih, C. F. and Needleman, A. (1985). A comparison of methods for calculating energy release rate. *Engng Fract. Mech.* **21**, 405–421.
- Nakamura, T. and Parks, D. M. (1988). Three-dimensional stress field near the crack front of a thin elastic plate. *J. Appl. Mech.* **55**, 805–813.
- Nakamura, T. and Parks, D. M. (1989). Antisymmetrical 3-D stress field near the crack front of a thin elastic plate. *Int. J. Solids Structures* **25**, 1411–1426.
- O'Dowd, N. P. and Shih, C. F. (1991). Family of crack-tip fields characterized by a triaxiality parameter: part I—structure of fields. *J. Mech. Phys. Solids* **39**, 989–1015.
- O'Dowd, N. P. and Shih, C. F. (1992). Family of crack-tip fields characterized by a triaxiality parameter: part II—fracture applications. *J. Mech. Phys. Solids* (accepted).
- Parks, D. M. (1991a). Three-dimensional aspects of HRR-dominance. In *Defect Assessment in Components—Fundamentals and Applications ESIS/EGF9* (Edited by J. G. Blauel and K.-H. Schwalbe), pp. 205–231. Mechanical Engineering Publications, London.
- Parks, D. M. (1991b). Engineering methodologies for assessing crack front constraint. *Proceedings, SEM Spring Conference on Experimental Mechanics*, June 10–13, 1991, pp. 1–8. Milwaukee, The Society for Experimental Mechanics, Inc., Bethel, CT.
- Raju, I. S. and Newman, J. C. (1979). Stress-intensity factors for a wide range of semielliptical surface cracks in finite thickness plates. *Int. J. Fract.* **29**, 817–829.
- Rice, J. R. (1974). Limitations to the small-scale yielding approximation for crack-tip plasticity. *J. Mech. Phys. Solids* **22**, 17–26.
- Sham, T.-L. (1991). The determination of the elastic  $T$ -term using higher order weight functions. *Int. J. Fract.* **48**, 81–102.
- Shih, C. F., Moran, B. and Nakamura, T. (1986). Energy release rate along a three-dimensional crack front in a thermally stressed body. *Int. J. Fract.* **30**, 79–102.
- Timoshenko, S. P. and Goodier, J. N. (1970). *Theory of Elasticity*. McGraw-Hill, New York.
- Wang, Y.-Y. (1991). On the two-parameter characterization of elastic–plastic crack front fields of surface-cracked plates. MIT Report, accepted for publication in ASTM Symposium on Crack Tip Constraint, Indianapolis, May, 1991.
- Wang, Y.-Y. and Parks, D. M. (1990). Evaluation of the elastic  $T$ -stress in surface-cracked plates using the line-spring method. MIT Report. *Int. J. Fract.* (accepted).
- Williams, M. L. (1957). On the stress distribution at the base of a stationary crack. *J. Appl. Mech.* **24**, 111–114.

APPENDIX

The interaction integral introduced in Section 2.2 may be generalized to cases where thermal strains and body forces are present. For isotropic linear isotropic elastic materials with a constant thermal expansion rate, the stress-strain relation is

$$\varepsilon_{ij} = \frac{1+\nu}{E} \sigma_{ij} - \frac{\nu}{E} \sigma_{kk} \delta_{ij} + \alpha \theta \delta_{ij}, \tag{A1}$$

where  $\alpha$  is the coefficient of thermal expansion and  $\theta$  is the temperature deviation from the reference value at undeformed state. Under presence of body force, the equilibrium condition is stated as,

$$\frac{\partial \sigma_{ij}}{\partial x_j} + b_i = 0, \tag{A2}$$

Here  $b_i$  is the body force per unit volume.

Starting from the interaction integral shown in (3) and invoking the divergence theorem, the expression for the interaction integral over a domain/volume can be expressed as

$$\bar{I}(s) = \int_{V(s)} \left[ \left( \sigma_{ij} \frac{\partial u_i^L}{\partial x_k} + \sigma_{ij}^L \frac{\partial u_i}{\partial x_k} \right) \frac{\partial q_k}{\partial x_j} - \sigma_{ij} \varepsilon_{ij}^L \frac{\partial q_k}{\partial x_k} + \left( \alpha \frac{\partial \theta}{\partial x_k} \sigma_{ii}^L - b_i \frac{\partial u_i^L}{\partial x_k} \right) q_k \right] dV. \tag{A3}$$

The derivation of (A3) is similar to the one given by Shih *et al.* (1986) for determining  $J$  in a thermally stressed body. Once  $\bar{I}$  is determined, the  $T$ -stress is obtained using (7) and (5).